Article

"Half-Sandwich"/Ru^II Anticancer Complexes Containing Triphenylphosphine and *p*-Substituted Benzoic Acids

João Honorato, [*,a] *Katia M. Oliveira,* [b] *Celisnolia M. Leite,* [a] *Legna Colina-Vegas,* [a,c] *Joaquim A. Nóbrega,* [a] *Eduardo E. Castellano,* [d] *Javier Ellena,* [d] *Rodrigo S. Correa* [b] *and Alzir A. Batista* [*,a,e]

ᵃDepartamento de Química, Universidade Federal de São Carlos (UFSCar), CP 676, 13561-901 São Carlos-SP, Brazil

ᵇDepartamento de Química, Instituto de Ciências Exatas e Biológicas (ICEB), Universidade Federal de Ouro Preto (UFOP), 35400-000 Ouro Preto-MG, Brazil

ᶜInstituto de Química, Universidade Federal do Rio Grande do Sul (UFRGS), 91501-970 Porto Alegre-RS, Brazil

ᵈInstituto de Física de São Carlos, Universidade de São Paulo (USP), CP 369, 13560-970 São Carlos-SP, Brazil

ᵉInstituto de Química, Universidade Federal de Goiás (UFG), 74690-900 Goiânia-GO, Brazil

Mononuclear and binuclear Ru^II/arene/triphenylphosphine complexes with *p*-substituted benzoic acid derivatives were prepared and characterized. These monocationic complexes of type [Ru(η^6-*p*-cymene)(PPh$_3$)L] (L = benzoic acid (**1**), *p*-hydroxybenzoic acid (**2**), *p*-nitrobenzoic acid (**3**) and terephthalic acid (**4**)) were characterized using various techniques, such as nuclear magnetic resonance (NMR) and matrix-assisted laser desorption/ionization-time of flight (MALDI-TOF) mass spectrometry, and the crystal structure of **1**, **3** and **4** were determined by X-ray diffraction analysis. The cytotoxicity of the complexes was evaluated, *in vitro*, against tumorigenic [MDA-MB-231, MCF-7 (breast), A549 (lung) and DU-145 (prostate)] and non-tumorigenic [MCF-10A (breast), MRC-5 (lung) and PNT-2 (prostate)] cells. The binuclear complex (**4**) was inactive due to its low solubility. Complexes **1**, **2** and **3** showed similar cytotoxicity, however, complex **1** presented better selectivity index against MDA-MB-231 than compounds **2** and **3**. Cellular ruthenium absorption was explored by inductively coupled plasma mass spectrometry (ICP-MS) analyzing the whole cells and the culture medium. Complementary studies showed that complex **1** inhibited colony formation, induced morphology changes in cells and promoted cell cycle arrest in the Sub-G1 phase for the MDA-MB-231 cells.

Keywords: piano-stool Ru^II complexes, benzoic acid analogs, antitumoral activity and cytotoxicity, cellular uptake

Introduction

In the medicinal inorganic chemistry field, research on new metal-based anticancer drugs has received considerable attention since the discovery of anticancer properties of cisplatin and analog drugs. Pt-based coordination compounds have been present in most conventional cancer treatments in recent years (40% approximately). Moreover, they are just as important now as they were when they first reached the market fifty years ago.[1,2] However, these drugs are restricted by severe dose-limiting due to side-effects. For instance, a cancer patient treated with platinum drugs can experience around 40 specific side-effects, such as severe nausea, vomiting and tissue damage as neurotoxicity, nephrotoxicity and others.[3-6] Ideally, an effective cancer drug is active against tumor cells not causing damage to healthy tissues. These facts are one of the most important motivator aspects to develop either new cisplatin analogs or other metal-based anticancer drugs. Recently, many tools have been used to develop new drugs/metallodrugs, such as those based on the structure-activity relationship (SAR),[7,8]

*e-mail: honoratoneto10@gmail.com; daab@ufscar.br
Dedicated to Prof Dr Henrique Eisi Toma on the occasion of his 70th birthday.

pharmacophore models,[9] pharmacokinetic approaches[10-12] and nanopreparations.[3,5,13,14]

In addition, another way to improve the metallodrugs used in the cancer treatment is to search for new active and selective complexes based on different metal centers. Among all the transition metals present in the periodic table, great emphasis has been given to the ruthenium complexes, which have a great structure variety. The first ruthenium complex with anticancer activity reported in the literature[15] was the *cis*-[Ru(NH$_3$)$_4$(Cl)$_2$]Cl (Figure 1), the cisplatin analog, for which the hypothesis of "activation-by-reduction" of Ru[III]/Ru[II] was suggested. This proposition was confirmed for one of the most studied ruthenium complexes, the NAMI-A (Figure 1), an efficient anti-metastatic drug. Alessio and co-workers[2] have demonstrated that to be active, *in vivo*, the NAMI-A acts as prodrugs under physiological conditions. Researchers[15-19] have suggested that the reduction of the Ru[III]/Ru[II] is important to produce a more labile complex, which rapidly reacts with specific sites of biomolecules, improving its antitumor activity.
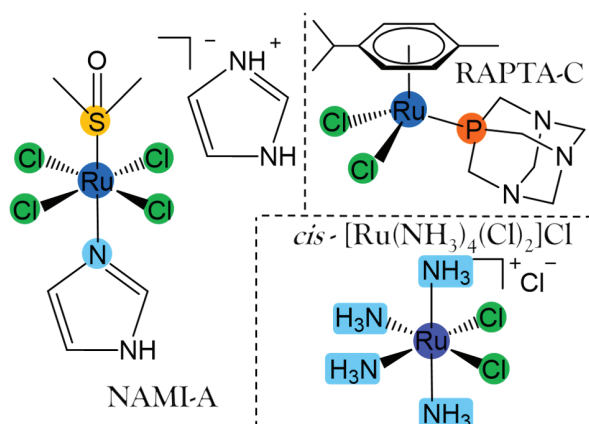

Figure 1. Chemical structures of the NAMI-A, RAPTA-C and *cis*-[Ru(NH$_3$)$_4$(Cl)$_2$]Cl complexes.

One specific class of ruthenium(II) compounds that has become very popular in recent years is the organometallic complexes of type "half-sandwich". Reports on Ru[II]/η[6]-arene complexes with the general formula [Ru(η[6]-arene)(L–L)(X)]^n can be found in the literature, where "L–L" (bidentate) and "X" (monodentate) are neutral or charged ligands of various types. Usually, X is a halide and, similar to NAMI-A, the activation of these complexes requires the hydrolysis of these ligands. However, the half maximal inhibitory concentration (IC$_{50}$) values in cancer cells for these compounds are generally high (> 100 μM), which is attributed to the high reactivity of these complexes, as a result of the low stability in organic solvents or under physiological conditions.[20-23] In addition, there are many

papers[22,23] which currently report the use of monophosphines or monopyridines as the "X" ligand, resulting in complexes with high toxicity (< 5 μM), thanks to the lipophilicity enhancement of the compounds, when at least one of these molecules is present in their structures. Furthermore, when "L–L" is N–N,[24-26] P–P,[27-32] N–S,[33,34] N–O,[24,31,32] O–O[24,35,36] donor ligand, a wide range of IC$_{50}$ values is obtained. Ruthenium arene 1,3,5-triaza-7-phosphaadamantane (RAPTA)-like (Figure 1) compounds are other groups of half-sandwich Ru[II] compounds that show good anticancer properties. Many of them present the phosphane ligand, known as PTA (1,3,5-triaza-7-phosphaadamantane), to form water-soluble complexes due to the high hydrophilic character of the PTA ligand. Thus, NAMI-A and RAPTA types of compounds exert an antimetastatic activity, and in parallel, present a good cytotoxic activity, and low toxicity, *in vivo*. This fact is surprising, considering the differences between the complexes in terms of ruthenium oxidation state, complex charge, ligands and geometry.

Concerning the O–O type of ligands coordinated in the bidentate form to the Ru[II]/η[6]-arene complex, it should be emphasized that the biological properties of carboxylate-based compounds are underexplored. Probably, the tensioned four-membered ring formed by metal/carboxylate anion moiety may present low stability when compared with the correspondent five/six-membered ones. Thus, the main problem of these kinds of Ru[II]/η[6]-arene/carboxylate complexes can be their low stability in coordinating solvents or physiological medium, limiting their biological application.[37,38] Benzoic acid and its analogs belong to an important class of ligands, displaying a structural diversity, allowing them to access the *ortho*, *meta* and *para* positions with a wide possibility of substitution with many organic functions. Due to the promising chemical and biological results obtained with the Ru[II]/η[6]-arene-based complexes, this paper reports on the reactivity of *p*-substituted benzoic acid derivatives with Ru[II]/η[6]-arene/triphenylphosphine complexes with general formula [Ru(η[6]-*p*-cymene)(PPh$_3$)(L$_3$)]BF$_4$ (benzoic acid (L$_1$); *p*-hydroxybenzoic acid (L$_2$); *p*-nitrobenzoic acid (L$_3$) and terephthalic acid (L$_4$)), in order to obtain active and stable compounds. The complexes were characterized by various techniques, such as Fourier transform infrared spectroscopy (FTIR), multinuclear nuclear magnetic resonance (NMR) spectroscopy and X-ray diffraction (XRD) experiments. Afterwards, the cytotoxicity of the complexes against four human tumor cell lines (MDA-MB-231/MCF-7 (breast), DU-145 (prostate) and A549 (lung)) and three non-tumor human cell lines (MRC-5 (lung), MCF-10A (breast) and PNT2 (prostate)) were evaluated. Therefore, to better understand the action mode of these complexes, we studied the cellular uptake

and cell death mechanism, including cell cycle disturbances and cell migration inhibition.

Results and Discussion

Synthesis and characterization

Four new complexes were synthesized from the reaction of the precursor complex [Ru(η^6-*p*-cymene)(PPh$_3$)Cl$_2$] with *para*-substituted benzoic acid derivatives, resulting in three mononuclear complexes and one binuclear, with a general formula [Ru(η^6-*p*-cymene)(PPh$_3$)(L)]BF$_4$ (**1**-**3**) and {[Ru(η^6-*p*-cymene)(PPh$_3$)]$_2$(μ-L$_4$)}(BF$_4$)$_2$ (**4**), respectively, as can be seen in Scheme 1. Pure products (**1**-**4**) were obtained when the syntheses were carried out using acetone as the solvent and silver salt (AgBF$_4$), in order to remove the chlorido ligand. This synthetic route contributes to forming ruthenium/carboxylate complexes with bidentate coordination mode (via O−O atoms). Other attempts to perform this synthesis, using weak (Et$_3$N) or strong (NaOH) bases as deprotonating agents, did not result in pure products. Thus, all complexes were isolated as tetrafluoroborate salts of the type 1:1 electrolyte, such as those supported by molar conductance measurements, in acetone solvent (59-188 S cm^2 mol^{-1}).

Alternatively, an attempt to obtain complex **1**, using sodium benzoate and [Ru(η^6-*p*-cymene)(PPh$_3$)Cl$_2$] in methanolic solution under reflux for 24 h, was monitored by ^{31}P{^{1}H} nuclear magnetic resonance. As a result, the formation of several by-products was observed, in which the most abundant one (occurring at 51.6 ppm in

^{31}P{^{1}H} NMR spectrum) was isolated by crystallization (methanol/hexane mixture 1:1 v/v). The crystal structure of this complex was determined by X-ray diffraction (Figure 2). Surprisingly, the arene ligand is absent in the complex. As confirmed by previous literature,[39,40] the reflux of ruthenium/arene complexes in methanolic solutions can promote the arene loss, making three coordination points available. As can be seen in Figure 2, the complex displays an interesting structural behavior observed for the first time. In addition to the coordinated water bridged between the ruthenium atoms, the structure obtained presented two triphenylphosphines (one coordinate for each ruthenium), one monodentate coordinated methanol molecule and four differently coordinated benzoates, resulting in a complex of formula [Ru$_2$(L$_1$)$_4$(CH$_3$OH)(PPh$_3$)$_2$(H$_2$O)], where L$_1$ = benzoic acid. The crystal structure displays the three possible coordination modes for carboxylate anion, monodentate, bidentate and bridging bidentate (see Figure 2). The absence of Ru^{III} signals in the electron paramagnetic resonance (EPR) spectrum confirms the oxidation state of the metal (Ru^{II}).

The single crystals of complexes **1**, **3** and **4** were obtained by slow evaporation of a dichloromethane solution. Complexes **1** and **3** crystallized with the addition of the KPF$_6$ salt, presenting the PF$_6^-$ as a counterion, while complex **4** crystallized with the original BF$_4^-$ counterion, with no need to add KPF$_6$ salt. The coordination mode of carboxylic acid to the metal as bidentate via O−O atoms was unambiguously confirmed by the X-ray technique, differing from the former binuclear structure with diverse coordination modes. The summary of crystal data and
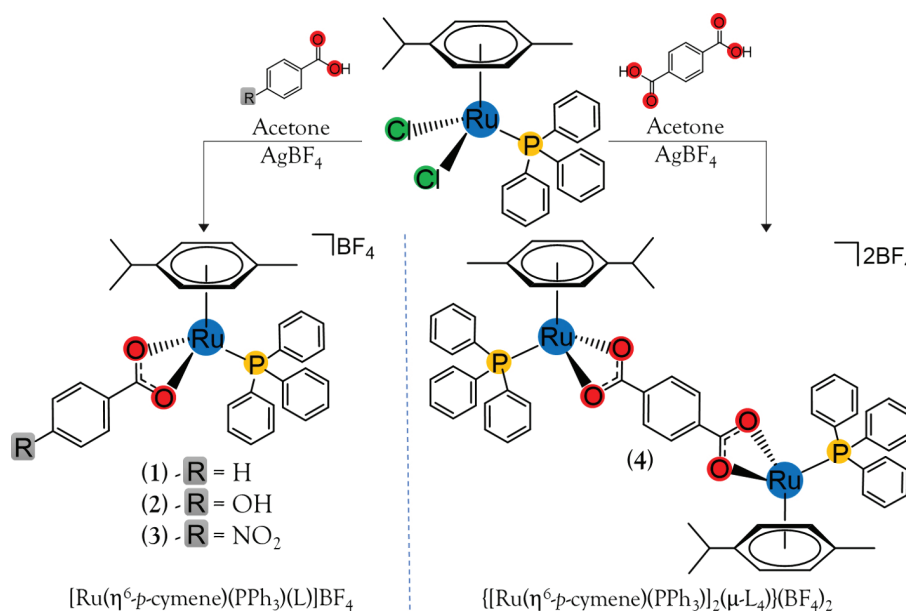
Scheme 1. Scheme for the synthesis of complexes **1**-**3** and **4** with the respective ligands: benzoic acid (L$_1$); *p*-hidroxybenzoic acid (L$_2$); *p*-nitrobenzoic acid (L$_3$) and terephthalic acid (L$_4$).
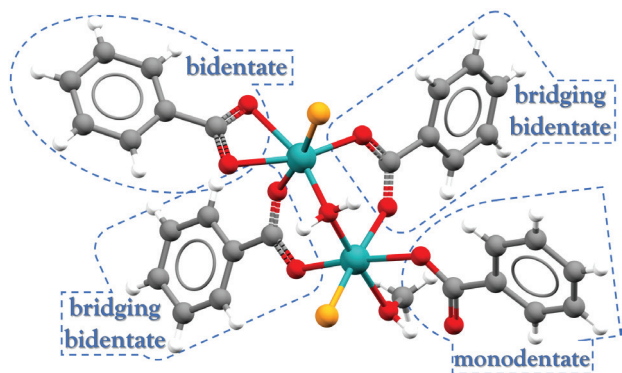
Figure 2. Crystal structure of the water bridged triphenylphosphine/ruthenium(II) benzoate complex of formula [Ru$_2$(L$_1$)$_4$(CH$_3$OH)(PPh$_3$)$_2$(H$_2$O)], where L$_1$ = benzoic acid. The triphenylphosphine rings were omitted to help visualize the molecule.

structural refinements are shown in the Supplementary Information (SI) section (Table S1). All complexes crystallized in a triclinic space group, in which complex **3** presents one molecule *per* asymmetric unit, complex **1** crystallizes with two equivalent molecules, while complex **4** shows one-half molecule being the complete structure generated by the inversion center located in the terephthalic ring.

All complexes present a "piano-stool" structure, displaying the ruthenium center in a pseudo-octahedral geometry, as can be seen in Figure 3. The six carbon atoms of the *p*-cymene ligand form the seat, whilst the three legs of the "piano-stool" are constituted by the phosphorus (triphenylphosphine) and oxygen atoms of carboxylate ion. The distorted geometry is confirmed by the P$_1$–Ru–O$_1$ and P$_1$–Ru–O$_2$ bond angles at around 90° and the low angle value for O$_1$–Ru–O$_2$ (near 60°), as expected, which occurs due to the high tensioned four-membered ring composed by the carboxylate group coordinated to the metal center. Selected bond lengths and bond angles are represented in Table 1. The bond lengths C$_1$–O$_2$ and C$_1$–O$_1$ differ from the free ligands due to the electron delocalization

between these chemical bonds after the deprotonation and subsequent coordination to the metal center. Thus, the C–O bond lengths are between the C=O double and C–O single bond lengths (Table 1).
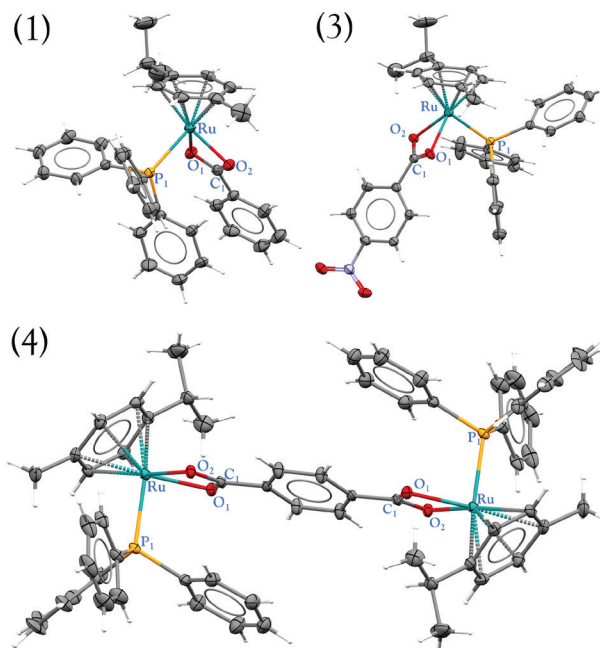

Figure 3. Crystal structures of complexes **1**, **3** and **4**. For the sake of clarity, the BF$_4^-$ or PF$_6^-$ counterions are not included. Thermal ellipsoids drawn at 30% probability.

The infrared (IR) spectra of the free *p*-substituted benzoic ligands exhibit the vO–H stretching vibrations in the range of 3700-3250 cm^{-1}, while in the spectra of the complexes (see Figure S22 of SI section) this band disappears due to the deprotonation and coordination of the carboxylate anion to the metal center, except for complex **2**, which has a *p*-substituted hydroxyl group. Another important change in the spectra of the complexes was the shift of the symmetric (v_{sym}COO$^-$) and asymmetric (v_{asy}COO$^-$) stretching of carboxylate anion, when

Table 1. Selected interatomic distances and bond angles for complexes **1**, **3** and **4** (L$_1$, L$_3$ and L$_4$ means data of the free carboxylate of the coordinated ligands)

	1	3	4	L$_1$	L$_3$	L$_4$
			Bond angle / degree			
O$_1$–Ru–O$_2$	61.32(7)	59.80(2)	60.84(2)	–	–	–
P$_1$–Ru–O$_2$	84.58(6)	90.41(9)	87.89(8)	–	–	–
P$_1$–Ru–O$_1$	92.25(5)	88.19(9)	85.79(8)	–	–	–
O$_1$–C$_1$–O$_2$	116.6(3)	117.7(4)	117.1(7)	123.6	123.5	123.47
			Bond length / Å			
Ru–O$_2$	2.123(9)	2.150(3)	2.114(6)	–	–	–
Ru–O$_1$	2.129(8)	2.141(3)	2.120(6)	–	–	–
Ru–P$_1$	2.385(7)	2.379(2)	2.363(2)	–	–	–
C$_1$–O$_1$	1.277(3)	1.248(5)	1.257(9)	1.252	1.232	1.252
C$_1$–O$_2$	1.272(3)	1.252(5)	1.256(7)	1.281	1.314	1.279

Table 2. Characteristic $v_{sym}COO^-$ and $v_{asy}COO^-$ stretching, $^{31}P\{^1H\}$ and ^{13}C selected NMR signals (CDCl$_3$) for complexes **1-4**

	$v_{asy}COO^{-a}$ / cm^{-1}	$v_{sym}COO^{-a}$ / cm^{-1}	Δv^a / cm^{-1}	δ $^{31}P\{^1H\}$ / ppm	δ ^{13}C of COO^{-a} / ppm
1	1596 (1602)	1481 (1413)	121 (140)	35.9	184.6 (176.4)
2	1602 (1612)	1479 (1416)	123 (132)	35.2	184.6 (171.1)
3	1593 (1618)	1477 (1390)	116 (187)	35.7	181.2 (173.7)
4	1567 (1627)	1471 (1394)	156 (173)	35.4	182.6 (176.1)

^{a}Free ligand values between parenthesis.

compared with the spectra of the free ligands. According to Honorato *et al.*[41] and Nakamoto,[42] complexes with COO$^-$ coordinated bidentate to the metal exhibit Δ value ($\Delta = v_{sym}COO^- - v_{asy}COO^-$) significantly lower than the values found for the free ligands. All complexes exhibit the same behavior, in which the $v_{sym}COO^-$ shift to high frequencies, and the $v_{asy}COO^-$ shift to low frequencies,[41,43-45] as can be seen in Table 2. Thus, the coordination of the carboxyl group to the ruthenium metal by bidentate mode can be also confirmed by IR spectra, as confirmed by X-ray crystallographic structures. An intense band near 1000 cm^{-1} in the complexes refers to vB−F, showing the presence of the BF$_4^-$ counter anion, as supported by molar conductance values. Weak intensity bands observed at around 495-501 and 336-377 cm^{-1} are assigned to vRu−P and vRu−O stretching vibrations, respectively.

All complexes were characterized by 1D multinuclear $^{31}P\{^1H\}$, ^1H, and $^{13}C\{^1H\}$ NMR experiments and by 2D correlation spectroscopy (COSY) (^1H-^1H), heteronuclear single quantum correlation (HSQC) (^{13}C-^1H) and heteronuclear multiple bond correlation (HMBC) (^{13}C-^1H). The $^{31}P\{^1H\}$ spectra of complexes display just one signal, a singlet for coordinated phosphorus of triphenylphosphine at around 35 ppm (see Table 2). As can be seen, the $^{31}P\{^1H\}$ signals in the complexes shifted to high frequencies when compared with the precursor [Ru(η^6-*p*-cymene)(PPh$_3$)Cl$_2$] (24 ppm) as a consequence of carboxylate coordination. The main cause of this deshielding effect on the phosphorus signal is the exchange of chlorido ligands (π- and σ-donor) by the carboxylate ligand (π-acceptor). ^1H and $^{13}C\{^1H\}$ NMR spectra of all synthesized complexes display the number of peaks according to the expected structures. In the ^1H NMR spectra of **1-4** (Figures S1, S6, S11 and S16 of SI section), three sets of signals were identified: the first one at low frequencies (δ 1-3 ppm) refers to the hydrogens of the methyl and propyl group of *p*-cymene. The second at around δ 5-6 ppm are signals assigned to the hydrogens of the ring of *p*-cymene, and the last refers to the hydrogens of triphenylphosphine and of *p*-substituted benzoic acids. All attributions were confirmed by the ^1H-^1H COSY experiment, showing the respective vicinal coupling of these chemical shifts.

A different displacement was observed for the hydrogens of *p*-substituted benzoic acid ring. The activating/deactivating effect of substituent exerts a direct influence on the chemical shift of these signals. As described in Figure 4, complex **3**, that contains the most deactivating group (NO$_2$ group) has the signal shifted to high frequencies (red arrow), while in complex **2**, with the most activating group (OH group), chemical shifts occur to lower frequencies (blue arrow). This effect is induced by the electron donation of the OH group, shielding the aromatic hydrogens, while the electron withdrawing effect of the NO$_2$ group deshields these signals.[46,47]
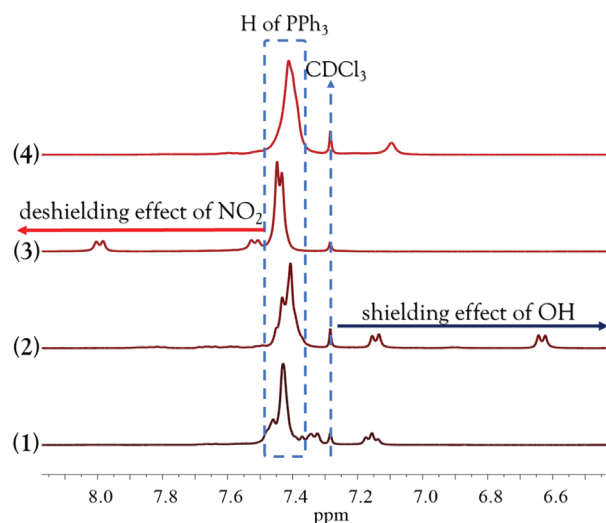

Figure 4. ^1H NMR spectra of complexes **1-4**, in CDCl$_3$, showing the peak displacement of hydrogen atoms of *p*-substituted benzoate ligands, bring on by the activating (blue arrow) and deactivating (red arrow) characteristics of *p*-substituents.

The ^{13}C NMR spectra of all complexes show one signal around 180 ppm, which is assigned to the carbon from the carboxylate group of the coordinated ligands. This deshielded signal, assigned to the coordinated carboxylate group, is far from that one observed in the free ligand (ca. 173 ppm) (Table 2). These results are in agreement with the literature report[41] that attributed this pronounced displacement to π-electron delocalization of the chelate ring formed after deprotonation and coordination, promoting a deshielding effect. This is also important evidence of the

metal coordination to the ligands through the carboxyl group. All the other signals were attributed using the 2D experiments (^{13}C-^{1}H HSQC and HMBC) (see the NMR spectra in the SI section, Figures S1 to S20).

The matrix-assisted laser desorption/ionization-time of flight mass spectra (MALDI-TOF-MS) for complexes **1**-**3** (see Figure S21 in the SI section) showed a signal corresponding to molecular mass without the tetrafluoroborate ion [M]$^{+}$ and the respective complex fragmentation, generating ions corresponding to the loss of *p*-substituted benzoate acid [M − L − H]$^{+}$ and coordination to the calibrant (dihydroxybenzoic acid, *m/z* 651.3). For complex **4**, the loss of one metal coordinate to the terephthalic acid generates the signal at *m/z*$^{+}$ 664.17 corresponding to the mononuclear complex [M + H]$^{+}$ and its fragmentation generates the same products observed for complexes **1**-**3**.

The stability of complexes **1**-**4** was studied using ^{31}P{^{1}H} NMR in acetone, dimethyl sulfoxide (DMSO) and in the mixture of these solvents with Roswell Park Memorial Institute (RPMI) biological medium (solvent/RPMI = 2:1). In DMSO and DMSO/RPMI, all compounds were not stable, forming several by-products from the labilization of the *p*-substituted benzoic acid or arene ligands, and were replaced by DMSO or chloride ions. This happened instantaneously after solubilization, as already described in the literature.[48] However, in the acetone/RPMI (2:1) mixture, the complexes were stable within the experiment time (48 h), displaying two signals at 0 ppm (phosphate of RPMI medium) and 34 ppm (complex **1**) (Figure 5). Previous reports[49,50] demonstrate that acetone was the most favorable solvent to dissolve compounds in cell growth *in vitro* experiments, displaying a non-toxic profile (0.1-1% v/v), which is a compatible solvent with the examined cells, as the MCF-7 studied in this work.
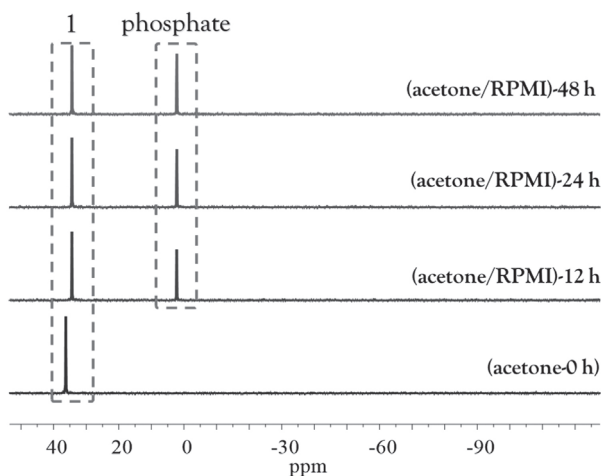

Figure 5. ^{31}P{^{1}H} NMR spectra of complex **1** (δ 35 ppm) in acetone/RPMI (2:1) at 0, 12, 24 and 48 h.

Biological anticancer experiments

The *in vitro* cytotoxicity assays of **1**-**4** and free ligands were carried out against four human tumor cell lines (MDA-MB-231/MCF-7 (breast), DU-145 (prostate) and A549 (lung)) and three non-tumor human cell lines (MRC-5 (lung), MCF-10A (breast) and PNT2 (prostate)), adopting a conventional tetrazolium colorimetric (3-(4,5-dimethylthiazol-2-yl)-2,5-diphenyltetrazolium bromide (MTT)) method. The IC$_{50}$ values and selective indexes (SI) are summarized in Table 3. The higher concentration tested for complex **4** was 30 μM, due to its low solubility. Under this condition, complex **4** does not display cytotoxic activity as it is inactive. On the other hand, complex **3** is more toxic than complexes **1**, **2** and the precursor. Given that complexes **1**, **2** and **3** were more cytotoxic than the respective precursor and free ligands for all evaluated cell lines, this suggests that the coordination of *p*-substituted benzoic acids to ruthenium may improve the cytotoxicity. As can be seen in Table 3, complex **1** was the most selective in all the tested cells, and was 3.5 times more active in the breast cancer cell MDA-MB-231 than the respective non-tumorigenic MCF-10A cells. These results are good evidence of the influence of the triphenylphosphine ligand on cellular toxicity. The literature[20-23] cites many examples of Ru^{II}-arene complexes, without phosphine, with very high IC$_{50}$ values in various tumorigenic cell lines. One of the causes that leads to low toxicity of these compounds is the lack of lipophilic groups, decreasing the cellular uptake of these complexes.[33,51,52]

To investigate the effects on cell morphology of the most selective compound, complex **1** was incubated with the MDA-MB-231 cells at different concentrations (Figure S23 of SI section) proportional to the IC$_{50}$ values. Negative control cells have a spindle-shaped phenotype in both strains, while cells treated with complex **1**, especially at 24 μM for MDA-MB-231 (2 × IC$_{50}$, 24 h), have spherically shaped cells (which may be indicative of apoptosis),[33,53-57] in addition to damaged cell bodies, ongoing cell death, loss of adhesion and confluence. For concentrations lower than IC$_{50}$, no considerable changes were observed, showing that complexes cannot cause visible damage at these concentrations.

The clonogenic assay is an *in vitro* cell survival test based on the ability of a single cell to proliferate retaining its reproductive ability to form a large colony (> 50 cells).[58,59] The colony area percentage, commonly associated with cell survival and colony intensity, shows the ability of the cells to grow in a densely populated colony. Complex **1** at a concentration of 6.0 μM (2 × IC$_{50}$) inhibited the number

**Table 3.** IC$_{50}$ values for **1-4** and cisplatin (CDDP) against DU-145 (human prostate cancer), A549 (human lung cancer), MDA-MB-231/MCF-7 (human breast cancer), MRC-5 (non-tumor human lung), PNT2 (non-tumor humam prostate) and MCF-10A (non-tumor human breast) cell lines with 48 h of incubation

	IC$_{50}$ / µM							Selectivity index[a]			
	MDA-MB-231	MCF-7	A549	DU-145	MCF-10A	MRC-5	PNT2	SI$_1$	SI$_2$	SI$_3$	SI$_4$
1	12.0 ± 0.7	19.3 ± 1.9	12.5 ± 0.8	15.5 ± 0.7	42.3 ± 7.0	20.1 ± 1.5	15.7 ± 2.2	3.5	2.2	1.6	1.0
2	12.8 ± 0.9	11.0 ± 0.5	11.5 ± 0.5	11.5 ± 0.5	18.1 ± 2.8	9.3 ± 2.0	6.1 ± 0.2	1.4	1.6	0.8	0.5
3	40.5 ± 4.0	49.9 ± 0.4	57.5 ± 2.8	60.7 ± 6.7	56.2 ± 2.2	35.9 ± 2.3	59.7 ± 5.8	1.4	1.1	0.6	0.9
4	> 30	> 30	> 30	> 30	> 30	> 30	> 30	–	–	–	–
Prec.	21.6 ± 1.3	18.2 ± 0.6	12.7 ± 1.2	49.7 ± 1.8	19.1 ± 1.0	50.6 ± 0.2	–	0.8	1.0	4.0	–
CDDP	2.4 ± 0.2	13.9 ± 2.0	14.4 ± 1.4	2.3 ± 0.4	29.4 ± 0.8	29.1 ± 0.8	21.4 ± 6.0	12	2.1	2.0	9.3

[a]SI$_1$ = MCF-10A/MDA-MB-231; SI$_2$ = MCF-10A/MCF-7; SI$_3$ = MRC-5/A549 and SI$_4$ = PNT2/DU-145. IC$_{50}$: half maximal inhibitory concentration; Prec.: [Ru(η^6-*p*-cymene)(PPh$_3$)Cl$_2$].

of colonies of MDA-MB-231 when compared to the control (Figure 6a). There was a concentration-response tendency, displaying the ability of **1** to perform cytotoxic and cytostatic effects, indicating the continuous loss of clonogenicity of MDA-MB-231 after the treatment. The metastatic process is a multiple step procedure, which includes clonogenic survival, angiogenic process, cell invasion and migration, resulting in a metastasis. Thus, MDA-MB-231, after exposed to **1** (48 h), diminished the ability of single cells (clones) to form colonies, demonstrating a very important property in therapy against metastatic cancer. Different from this, a large number of reports[33,41,60-63] demonstrate the ability of ruthenium-based complexes to eliminate the clonogenicity at low concentrations, not exhibiting a concentration-response tendency.

Cell migration is an important step of angiogenesis, which is associated to the metastasis. The ability of **1** to inhibit the migration of MDA-MB-231 cells was evaluated by the wound healing assay (Figure 7a). Different from the control, where the cells spontaneously migrated until complete wound closure after 48 h, complex **1** decreased the migration capacity of breast tumor cells, observing the existence of the wound after 48 h of cell treatment with **1**. At 24 h, the statistical analysis shows a concentration-response tendency (Figure 7a), confirming the anti-migratory properties of complex **1**. The cell cycle progression of MDA-MB-231 cells, under treatment with **1**, was evaluated by flow cytometry. Results show cell accumulation in the Sub-G1 phase at concentrations greater than the IC$_{50}$ value, showing no significant changes in concentrations less than
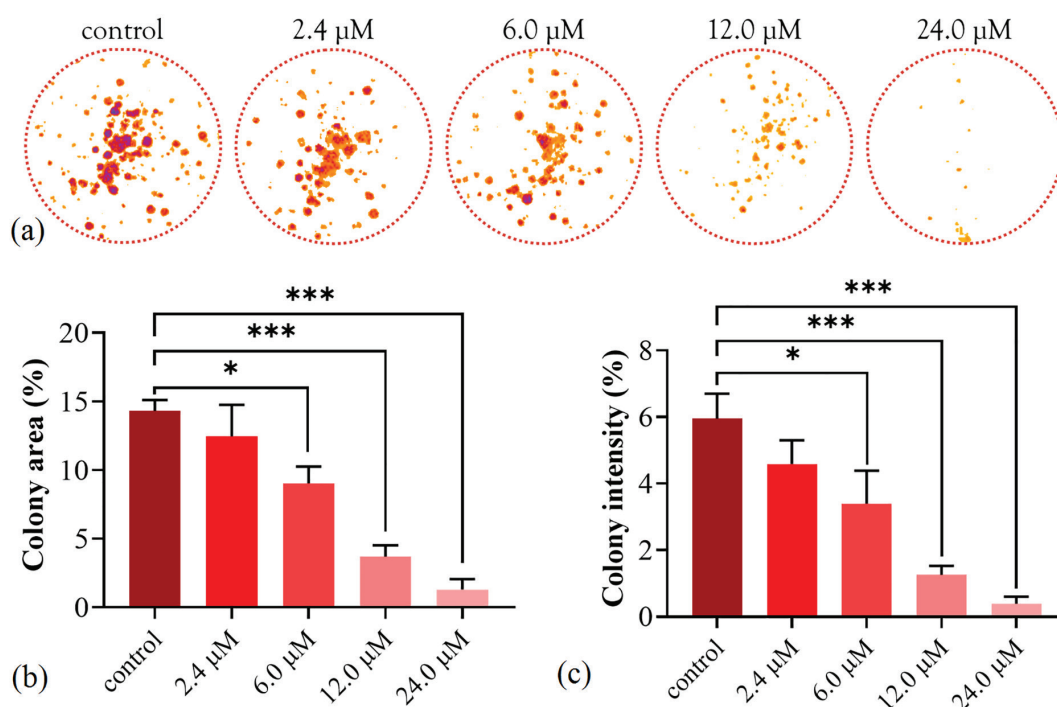
Figure 6. Colony formation (a) and quantification of colony area (b) and intensity (c). Significant at the *$p < 0.05$ and *** $p < 0.001$ levels using analysis of variance (ANOVA).

or equal to the IC$_{50}$, as compared to the control, as shown in Figure 7b. This result is consistent with the cytotoxic activity of complexes in MDA-MB-231 cells. Inhibition at the Sub-G1 stage indicates apoptosis cell death by DNA cleavage or by an indirect route. For the concentrations lower than the IC$_{50}$, corroborating with the morphological observations, no cell cycle arrest was observed.
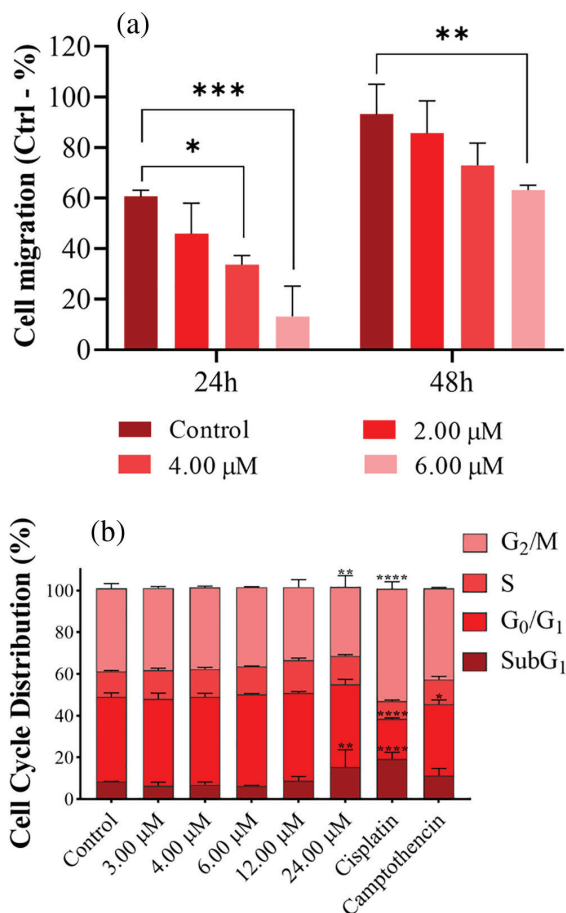

Figure 7. (a) Quantitative analysis of the cell migration by measuring the cell wounded region; (b) effect of complex **1** on the MDA-MB-231 cell cycle distribution analyzed by flow cytometry. Significant at the *$p < 0.05$, **$p < 0.01$, ***$p < 0.0001$ and ****$p < 0.0001$ levels using analysis of variance (ANOVA).

The ruthenium concentration was determined by inductively coupled plasma mass spectrometry (ICP-MS) in adherent tumor cells MDA-MB-231, in the initial and final culture medium. Figure 8 shows the ^{102}Ru concentration, expressed in µg L^{-1}, for the treated cells and for the exposed media. As can be seen, the adherent tumor cells showed approximately 30% of cellular uptake in relation to the initial culture medium. The remaining ruthenium concentration was found in the final culture medium. The analyte concentrations, determined in the samples, did not present significant differences (*t*-paired test with 95% of confidence). The average concentration

of Ru after 24 h of incubation with complex **1** was 250 ± 16 fg *per* MDA-MB-231 cell. Our results are in agreement with previous publications[64-66] regarding ruthenium uptake in tumor cell lines. The published results revealed an average of 0.9 fg of Ru *per* A2780 cell incubated with RAPTA-C,[64] 30 fg of Ru *per* SW180 cell incubated with the compound *trans*-[tetrachlorobis(1*H*-indazole) ruthenate(III)] (KP1019)[65] and 206-298 fg of Ru *per* A459 cell, incubated with Ru methylimidazole complexes.[66]
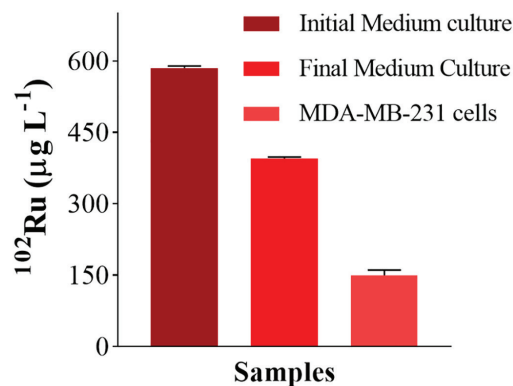

Figure 8. Ruthenium concentrations in culture medium and adherent tumor cells MDA-MB-231. Cells cultured with 5 µM of complex **1** for 24 h. Error bars represent the standard deviation of three experimental (cell flask) replicates.

Conclusions

Four new [Ru(η^6-*p*-cymene)(PPh$_3$)(O−O)] complexes, where O−O = *p*-substituted benzoic acids, were synthesized, characterized and their cytotoxicity activities were evaluated against the MDA-MB-231, MCF-7 (breast), DU-145 (prostate) and A549 (lung) tumor cells and in the non-tumor MCF-10A (breast), MRC-5 (lung) and PNT2 (prostate) cells. Except for the binuclear complex **4** (insoluble in the biological medium), all the complexes were cytotoxic for tumor cells, but complex **1** was more selective on the breast cell line MDA-MB-231. Complex **1** is able to inhibit colony formation and cell migration, with considerable concentration-response tendency. In addition, complex **1** does not interfere with cell cycle and morphology at concentrations below IC$_{50}$ values, and accumulates in MDA-MB-231 cells, as shown in cellular uptake experiments. However, additional studies need to be performed, both *in vivo* and *in vitro*, to effectively understand the mechanisms of action that promote selective tumor cell death.

Experimental

The precursors [Ru(η^6-*p*-cymene)(PPh$_3$)Cl$_2$] and [Ru(η^6-*p*-cymene)Cl$_2$]$_2$ were synthesized according to

previous works related in the literature.[67,68] All solvents and reagents employed in this work presented analytical grade and were purchased from Sigma-Aldrich Brazil (Cotia, São Paulo, Brazil). Aqueous solutions were prepared with pure water produced by Milli-Q water (18.2 MΩ cm, Millipore, Billerica, United States) system.

General procedure

In a dark room, the [Ru(η⁶-*p*-cymene)(PPh₃)Cl₂] (0.180 mmol; 0.100 g) was dissolved in 15 mL of acetone for subsequent addition of the respective *p*-substituted benzoic acid ligand (0.198 mmol for **1-3**, 0.090 mmol for **4**) and (0.378 mmol) of AgBF₄. The mixture was kept under inert atmosphere and was stirred for 1.0 h, then this solvent was evaporated. 15 mL dichloromethane was added and filtered off in a Celite column. The resulting solution was dried under reduced pressure solubilized in 2 mL of methanol and precipitated with the addition of distilled water. The solid was filtered off, washed with water (3 × 5 mL) and dried under vacuum.

[Ru(η⁶-*p*-Cymene)(PPh₃)(L₁)]BF₄ (**1**)

Yield: 95 mg (78%); anal. calcd. for $C_{35}H_{34}B_1F_4O_2P_1Ru_1$: C, 59.59; H, 4.86%; found: C, 59.55; H, 4.81%; molar conductance (CH₃OH) / (S cm² mol⁻¹) 25.2; IR (KBr) ν / cm⁻¹ 1602 ($v_{asy}COO^-$), 1481 ($v_{sym}COO^-$), 1436 (*v*C=C), 1064 (*v*P−CH and *v*B−F), 526 (*v*Ru−P), 460 (*v*Ru−O); MALDI-TOF-MS *m/z*, calcd. for $C_{35}H_{34}O_2P_1Ru_1$ [M]⁺: 619.134, found: 619.080; ³¹P NMR (161.976 MHz, CDCl₃, 298 K) δ 35.59 (s); ¹H NMR (400.132 MHz, CDCl₃, 298 K) δ 7.46-7.36 (16H, m, 15H, rings of PPh₃ + 1H, *para* of benzoic acid), 7.31 (2H, d, *ortho* of benzoic acid), 7.26 (CDCl₃), 7.13 (2H, t, *meta* of benzoic acid), 5.80 (2H, d, *ortho* of *p*-cymene), 5.70 (2H, *meta* of *p*-cymene), 2.56 (1H, m, CH of propyl), 1.99 (3H, s, *para* CH₃ of *p*-cymene), 1.25 (6H, d, CH₃ of propyl); ¹³C NMR (100.62 MHz, CDCl₃) δ 184.22 (COO⁻_coord of lig), 134.60-127.55 (CH of lig and rings of PPh₃), 106.23, 95.85, 86.89 (ring of *p*-cymene), 31.76 (CH of propyl), 22.24 (CH₃ of propyl), 18.48 (CH₃ of *p*-cymene).

[Ru(η⁶-*p*-Cymene)(PPh₃)(L₂)]BF₄ (**2**)

Yield: 105 mg (83%); anal. calcd. for $C_{35}H_{34}B_1F_4O_3P_1Ru_1$: C, 58.26; H, 4.75%; found: C, 58.49; H, 4.97%; molar conductance (CH₃OH) / (S cm² mol⁻¹) 22.5; IR (KBr) ν / cm⁻¹ 3410 (*v*OH), 1602 ($v_{asy}COO^-$), 1479 ($v_{sym}COO^-$), 1436 (*v*C=C), 1087 (*v*P−CH and *v*B−F), 526 (*v*Ru−P), 453 (*v*Ru−O); MALDI-TOF-MS *m/z*, calcd. for $C_{35}H_{34}O_3P_1Ru_1$ [M]⁺: 635.129, found: 635.263; ³¹P NMR (161.976 MHz, CDCl₃, 298 K) δ 35.17 (s); ¹H NMR (400.132 MHz, CDCl₃,

298 K) δ 7.43-7.37 (15H, m, rings of PPh₃), 7.26 (CDCl₃), 7.12 (2H, d, *ortho* of *p*-hydroxybenzoic acid), 6.61 (2H, d, *meta* of *p*-hydroxybenzoic acid), 5.67 (2H, d, *ortho* of *p*-cymene), 5.56 (2H, *meta* of *p*-cymene), 2.53 (1H, m, CH of propyl), 1.96 (3H, s, *para* CH₃ of *p*-cymene), 1.21 (6H, d, CH₃ of propyl); ¹³C NMR (100.62 MHz, CDCl₃) δ 184.76 (COO⁻_coord of lig), 162.02 (C *para*, of lig), 134.59-114.92 (CH of lig and rings of PPh₃), 106.16, 95.57, 86.03 (ring of *p*-cymene), 31.70 (CH of propyl), 22.25 (CH₃ of propyl), 18.42 (CH₃ of *p*-cymene).

[Ru(η⁶-*p*-Cymene)(PPh₃)(L₃)]BF₄ (**3**)

Yield: 110 mg (83%); anal. calcd. for $C_{35}H_{33}B_1F_4N_1O_4P_1Ru_1$: C, 56.01; H, 4.43; N, 1.87%; found: C, 55.56; H, 4.94; N, 1.89%; molar conductance (CH₃OH) / (S cm² mol⁻¹) 12.4; IR (KBr) ν / cm⁻¹ 1627 ($v_{asy}COO^-$), 1523 ($v_{asy}NOO$), 1477 ($v_{sym}COO^-$), 1438 (*v*C=C), 1384 ($v_{sym}NOO$), 1087 (*v*P−CH and *v*B−F), 524 (*v*Ru−P), 460 (*v*Ru−O); MALDI-TOF-MS *m/z*, calcd. for $C_{35}H_{33}N_1O_4P_1Ru_1$ [M]⁺: 664.119, found: 664.160; ³¹P NMR (161.976 MHz, CDCl₃, 298 K) δ 35.73 (s); ¹H NMR (400.132 MHz, CDCl₃, 298 K) δ 7.97 (2H, d, *meta* of *p*-nitrobenzoic acid), 7.49 (2H, d, *ortho* of *p*-nitrobenzoic acid), 7.42 (15H, m, rings of PPh₃), 7.26 (CDCl₃), 5.80 (2H, d, *ortho* of *p*-cymene), 5.72 (2H, *meta* of *p*-cymene), 2.54 (1H, m, CH of propyl), 2.01 (3H, s, *para* CH₃ of *p*-cymene), 1.24 (6H, d, CH₃ of propyl); ¹³C NMR (100.62 MHz, CDCl₃) δ 181.37 (COO⁻_coord of lig), 150.38 (C *para* of lig), 134.59-122.83 (CH of lig and rings of PPh₃), 105.69, 95.68, 87.02 (ring of *p*-cymene), 31.77 (CH of propyl), 22.19 (CH₃ of propyl) and 18.52 (CH₃ of *p*-cymene).

{[Ru(η⁶-*p*-Cymene)(PPh₃)]₂(μ-L₄)}(BF₄)₂ (**4**)

Yield: 80 mg (63%); anal. calcd. for $[C_{64}H_{62}B_2F_8O_4P_2Ru_2].H_2O$: C, 56.90; H, 4.78%; found: C, 56.79; H, 4.43%; molar conductance (CH₃OH) / (S cm² mol⁻¹) 50.3; IR (KBr) ν / cm⁻¹ 1608 ($v_{asy}COO^-$), 1471 ($v_{sym}COO^-$), 1525, 1427 (*v*C=C), 1047 (*v*P−CH and *v*B−F), 516 (*v*Ru−P), 449 (*v*Ru−O); MALDI-TOF-MS *m/z*, calcd. for $C_{36}H_{34}O_4P_1Ru_1$ [M − [Ru(*p*-cymene)(PPh₃)] + H]⁺: 664.130, found: 664.160; ³¹P NMR (161.976 MHz, CDCl₃, 298 K) δ 35.42 (s); ¹H NMR (400.132 MHz, CDCl₃, 298 K) δ 7.42-7.37 (30H, m, rings of 2PPh₃), 7.26 (CDCl₃), 7.08 (4H, d, ring of terephthalic acid), 5.72 (4H, m, ring of *p*-cymene), 2.53 (2H, m, CH of propyl), 2.02 (6H, s, *para* CH₃ of *p*-cymene), 1.22 (12H, d, CH₃ of propyl); ¹³C NMR (100.62 MHz, CDCl₃) δ 182.65 (COO⁻_coord of lig), 134.60-127.14 (CH of lig and rings of PPh₃), 105.49, 95.79, 87.16 (ring of *p*-cymene), 31.74 (CH of propyl), 22.25 (CH₃ of propyl) and 18.60 (CH₃ of *p*-cymene).

Instrumentation

All manipulations were carried out under an argon atmosphere using standard Schlenk techniques. The microanalyses were performed using a FISIONS CHNS, model EA 1108. The IR spectra were recorded on a FTIR Bomem-Michelson 102 spectrometer in the 4000-250 cm^{-1} region, in KBr pellets. Conductivity values were obtained using a Meter Lab CDM2300 instrument. The MALDI-TOF-MS experiments were performed adopting the MALDI-TOF/TOF Bruker Daltonics Autoflex Speed mass spectrometer equipment, using dihydroxybenzoic acid as a calibrator. The NMR experiments (^{1}H, ^{13}C{^{1}H}, ^{31}P{^{1}H}, ^{1}H-^{1}H COSY, ^{1}H-^{13}C HSQC and ^{1}H-^{13}C HMBC) were recorded on a Bruker DRX 400 Ultrashield ™ (400.132 MHz for hydrogen frequency, 100.623 MHz for carbon frequency and 161.976 MHz for phosphorus frequency), referenced with TMS (tetramethylsilane). For all NMR experiments, 15 mg complexes were dissolved in deuterated chloroform (CDCl$_3$-*d*, Cambridge Isotope Laboratories, Inc., USA). ^{31}P{^{1}H} experiments are reported in relation to H$_3$PO$_4$ (85% v/v) and performed in acetone or reaction medium, using a capillary containing D$_2$O. The ^{31}P{^{1}H} registered spectra for the stability studies employing as solvents acetone (67%) and RPMI (33%) supplemented with fetal bovine serum (FBS, 10%).

X-ray structure determination

Complexes **1**, **3** and **4** were crystallized from methanolic solution resulting in red single crystals. The measurements of a single crystal by X-ray diffraction were performed on a Rigaku XtaLAB mini II or APEX DUO (Bruker) diffractometer with graphite monochromator and Mo Kα radiation (λ = 0.71073 Å). The structures were obtained by the intrinsic phasing method using SHELXT.[69] The Gaussian method was used for the absorption corrections. The table and structure representations were generated by OLEX2[70] and MERCURY,[71] respectively. The main crystal data collections and structure refinement parameters for all complexes are summarized in the SI section (Table S1).

Biological experiments

MDA-MB-231 (ATCC No. HTB-26) human breast tumor cells, A549 (ATCC No. CCL-185) human lung tumor cells and MRC-5 (ATCC No. CCL-171) non-tumor human lung cells were maintained in Dulbecco's modified Eagle's medium (DMEM) containing 10% of FBS. DU-145 (ATCC No. HTB-81) human prostate tumor cells and PNT2

non-tumor human prostate cells were maintained in the RPMI-1640 medium also supplemented with 10% of FBS. The non-tumor human breast cell line, MCF-10A (ATCC No. CRL-10317), was cultivated in DMEM/F12 medium containing 5% of horse serum, epidermal growth factor (EGF) (0.02 mg mL^{-1}); hydrocortisone (0.05 mg mL^{-1}); cholera toxin (0.001 mg mL^{-1}); insulin (0.01 mg mL^{-1}); penicillin (100 UI mL^{-1}); streptomycin (100 mg mL^{-1}) and L-glutamine (2 mM). All cell lines were maintained at 37 °C in a humidified 5% CO$_2$ atmosphere. For cell viability assay by the MTT method, 1.5×10^4 cells well^{-1} were seeded in 150 μL of the supplemented medium into 96-well plates. After 24 h, the cells were treated with different concentrations of the complexes (dissolved in acetone, final concentration of 1% v/v) and incubated for 48 h. MTT (1 mg mL^{-1}) was added (30 μL well^{-1}) and the plates were incubated again for 4 h. After removing the medium, the formazan crystals were dissolved in isopropanol. Negative control experiments were loaded with the addition of acetone (1%). The optical density was measured at 540 nm using a 96-well multiscanner autoreader (ELISA).

Cell morphology

MDA-MB-231 or MCF-10A cells were seeded (10.5×10^5 cells well^{-1}) in a 12-well plate and incubated in the supplemented medium at 37 °C in 5% CO$_2$ for 24 h. Cell morphology was examined after treatment of the cells with different concentrations of complexes for 48 h, in an inverted microscope (Nikon, T5100) with amplification of 10× of magnification.

Colony formation

A density of 300 cells well^{-1} of the MDA-MB-231 cell line was seeded into a 6-well plate and maintained in the supplemented medium at 37 °C in 5% CO$_2$ for 24 h. Cells were treated with different concentrations of the complexes for 48 h. The medium was replaced by a fresh medium without any complex and the plates incubated for 10 days. The cells were washed with phosphate-buffered saline (PBS), fixed with methanol and acid acetic (3:1) for 5 min and stained with Panotic dye for 5 min. Relative survival was calculated from the number of single cells that formed colonies (aggregate of at least 50 cells).

Migration

In the wound healing assay, MDA-MB-231 cells (0.5×10^5 well^{-1}) were plated in 12-well plates and incubated until the culture reached around 90% of confluence. A straight scratch was made with a sterile pipette tip and cells were washed with PBS and fresh medium. Cells were incubated with the complex (lower

than IC_{50}). Images were taken using a Moticam, 1000-S camera coupled to an inverted microscope (Nikon, T5100) at 4× total magnification at 0 and 24 h. For the transwell assay, a density of 0.5×10^5 cells well^{-1} of MDA-MB-231 was incubated with complexes, in different concentrations, and seeded on the upper chamber in a DMEM medium without FBS. In the lower chamber, DMEM medium with 10% FBS was added. The eventual migration process occurred for 22 h at 37 °C in 5% CO_2. Cells that remained in the upper chamber were removed with a cotton swab and cells that migrated through the upper chamber membrane were fixed with methanol and stained with 1% toluidine blue. Migrated cells were quantified by manual counting.

Cell cycle analysis

Flow-cytometric analysis of the cell cycle phase distribution of MDA-MB-231 cells, treated with ruthenium complex, was carried out seeding the quantity of 4.0×10^5 cells well^{-1}, in 6-well plates in DMEM/10% FBS medium. The cells were incubated at 37 °C in a humidified 5% CO_2 atmosphere for 24 h and treated with different concentrations of complexes and camptothecin (positive control). After 48 h of incubation, the cells were collected, washed with PBS and resuspended in 70% ice cold ethanol and frozen at −20 °C for 12 h. After this period, the cells were centrifuged and resuspended in a solution of RNase A (0.02 mg mL^{-1}) and propidium iodide (PI) (1 µg mL^{-1}) in PBS, incubated at 37 °C for 30 min and the DNA content was determined by flow cytometry. The experiment was performed in triplicate.

Cellular uptake experiments

One day before the treatment, 1.5×10^6 MDA-MB-231 cells were seeded in a Corning Costar 125 cm^2 flask. The medium was replaced with a new one containing 5 µM of complex **1** and incubated with the cells for 24 h at 37 °C. A separate flask with medium free metal was used as the control. At the end of the incubation period, the medium was transferred to a pre-cleaned tube, centrifuged (1200 rpm, 5 min) to remove floating cells, and the supernatant was collected for further analysis. The cells were washed twice with 10 mL of ice-cold ultrapure water, trypsinized with 4.0 mL trypsin-ethylenediamine tetraacetic acid (EDTA) solution for 2 min, and 6 mL of culture medium was added. Then, the cell suspension was transferred to a pre-cleaned tube, centrifuged (1200 rpm, 5 min, 2 °C), and the supernatant solution was carefully removed using a pipette. Finally, the cells were washed with 2 mL of cooled ultrapure water, pelleted, and stored at −20 °C for further analysis.

ICP-MS measurements

Ultrapure water (resistivity ≥ 18.2 MΩ cm at 25 °C) obtained from a Milli-Q Element water purification system (Merck Millipore, Bedford, MA, USA) was used throughout. HNO_3 (14 M) for trace metal analysis was previously purified by sub-boiling distillation in a Distillacid™ BSB-939-IR apparatus (Berghof, Eningen, Germany). Tetramethylammonium hydroxide solution (TMAH, Sigma-Aldrich Brazil, Cotia, São Paulo, Brazil) 25% was used as received. All determinations of metal content were conducted by monitoring the ^{102}Ru signal on an ICP-MS Agilent 7800 equipped with a concentric nebulizer and a Scott double pass spray chamber. A single-element Ru standard solution used for ICP-MS calibrations was prepared by diluting 1000 mg L^{-1} of Ru (Qhemis, São Paulo, SP, Brazil) in 0.14 mol L^{-1} HNO_3 medium, as well as Rh and Ir used as internal standards. The analytical solutions for calibration contained from 0.010 to 200 µg L^{-1} of each analyte and the internal standards were added at 10.0 µg L^{-1} to analytical calibration solutions, analytical blanks and samples. Cell pellets were digested using 200 µL of TMAH and acidified with 200 µL of HNO_3. Subsequently, the digests were diluted with water to 5% v/v HNO_3. The culture medium was digested using 1 mL of the initial or final medium and 250 µL of HNO_3 directly in the perfluoroalkoxy alkane (PFA) digestion vessels and microwave-assisted digested using a single reaction chamber oven (UltraWave™, Milestone, Sorisole, Italy). The chamber was pressurized with nitrogen gas (99.9%, White Martins, Praxair) to 40 bar. The microwave heating program was applied as follows: (*i*) 10 min to reach 180 °C and (*ii*) 10 min to hold it at 180 °C. Subsequently, digests were diluted to 20.0 mL with distilled-deionized water and an aliquot of each solution was appropriately 50-fold diluted, followed by quantification by ICP-MS. The initial and the final cultured mediums are defined as the medium prepared with 5 µM of complex **1**, before and after the cellular exposition.

Supplementary Information

CCDC codes: 1974084 (**1**), 1974085 (**3**), 1974086 (**4**) and 1974087 (**5**) contain the supplementary crystallographic data for this paper. These data can be obtained free of charge from The Cambridge Crystallographic Data Centre via www.ccdc.cam.ac.uk/data_request/cif.

Supplementary data (NMR, XRD, FTIR and MALDI-TOF spectra) are available free of charge at http://jbcs.sbq.org.br as PDF file.

Acknowledgments

Author Contributions

João H. A. Neto was responsible for the conceptualization, formal analysis, investigation, writing original draft, review and editing; Katia M. Oliveira, Celisnolia M. Leite, Legna Colina-Vegas for the investigation and writing original draft; Joaquim A. Nóbrega, Eduardo E. Castellano, Javier Ellena for the formal analysis and resources; Rodrigo S. Correa for the conceptualization, formal analysis, writing original draft, review and editing; Alzir A. Batista for the conceptualization, formal analysis, funding acquisition, project administration, resources, writing original draft, review and editing.

References

1. http://theconversation.com/happy-50th-anniversary-to-cisplatin-the-drug-that-changed-cancer-treatment-38382, accessed in April 2020.

2. Simović, A. R.; Masnikosa, R.; Bratsos, I.; Alessio, E.; *Coord. Chem. Rev.* **2019**, *398*, ID 113011.

3. Barabas, K.; Milner, R.; Lurie, D.; Adin, C.; *Vet. Comp. Oncol.* **2008**, *6*, 1.

4. Miller, R. P.; Tadagavadi, R. K.; Ramesh, G.; Reeves, W. B.; *Toxins (Basel)* **2010**, *2*, 2490.

5. Amable, L.; *Pharmacol. Res.* **2016**, *106*, 27.

6. Oun, R.; Moussa, Y. E.; Wheate, N. J.; *Dalton Trans.* **2018**, *47*, 6645.

7. Sarmah, P.; Deka, R. C.; *J. Comput.-Aided Mol. Des.* **2009**, *23*, 343.

8. Varbanov, H. P.; Jakupec, M. A.; Roller, A.; Jensen, F.; Galanski, M.; Keppler, B. K.; *J. Med. Chem.* **2013**, *56*, 330.

9. Pagano, N.; Maksimoska, J.; Bregman, H.; Williams, D. S.; Webster, R. D.; Xue, F.; Meggers, E.; *Org. Biomol. Chem.* **2007**, *5*, 1218.

10. Andersson, A.; Fagerberg, J.; Lewensohn, R.; Ehrsson, H.; *J. Pharm. Sci.* **1996**, *85*, 824.

11. Urien, S.; Lokiec, F.; *Br. J. Clin. Pharmacol.* **2004**, *57*, 756.

12. Farris, F. F.; Dedrick, R. L.; King, F. G.; *Toxicol. Lett.* **1988**, *43*, 117.

13. Alam, N.; Qayum, A.; Kumar, A.; Khare, V.; Sharma, P. R.; Andotra, S. S.; Singh, S. K.; Koul, S.; Gupta, P. N.; *Mater. Sci. Eng., C* **2016**, *68*, 109.

14. Cheng, Y.; Zhao, P.; Wu, S.; Yang, T.; Chen, Y.; Zhang, X.; He, C.; Zheng, C.; Li, K.; Ma, X.; Xiang, G.; *Int. J. Pharm.* **2018**, *545*, 261.

15. Reisner, E.; Arion, V. B.; da Silva, M. F. C. G.; Lichtenecker, R.; Eichinger, A.; Keppler, B. K.; Kukushkin, V. Y.; Pombeiro, A. J. L.; *Inorg. Chem.* **2004**, *43*, 7083.

16. Clarke, M. J.; *Coord. Chem. Rev.* **2002**, *232*, 69.

17. Sava, G.; Gagliardi, R.; Bergamo, A.; Alessio, E.; Mestroni, G.; *Anticancer Res.* **1999**, *19*, 969.

18. Reisner, E.; Arion, V. B.; Keppler, B. K.; Pombeiro, A. J. L.; *Inorg. Chim. Acta* **2008**, *361*, 1569.

19. Jakupec, M. A.; Reisner, E.; Eichinger, A.; Pongratz, M.; Arion, V. B.; Galanski, M.; Hartinger, C. G.; Keppler, B. K.; *J. Med. Chem.* **2005**, *48*, 2831.

20. Pantić, D. N.; Mihajlović-Lalić, L. E.; Aranđelović, S.; Radulović, S.; Grgurić-Šipka, S.; *J. Coord. Chem.* **2019**, *72*, 908.

21. Jeyalakshmi, K.; Haribabu, J.; Balachandran, C.; Swaminathan, S.; Bhuvanesh, N. S. P.; Karvembu, R.; *Organometallics* **2019**, *38*, 753.

22. Renfrew, A. K.; Karges, J.; Scopelliti, R.; Bobbink, F. D.; Nowak-Sliwinska, P.; Gasser, G.; Dyson, P. J.; *ChemBioChem* **2019**, *20*, 2876.

23. Deacon-Price, C.; Romano, D.; Riedel, T.; Dyson, P. J.; Blom, B.; *Inorg. Chim. Acta* **2019**, *484*, 513.

24. Habtemariam, A.; Melchart, M.; Fernández, R.; Parsons, S.; Oswald, I. D. H.; Parkin, A.; Fabbiani, F. P. A.; Davidson, J. E.; Dawson, A.; Aird, R. E.; Jodrell, D. I.; Sadler, P. J.; *J. Med. Chem.* **2006**, *49*, 6858.

25. Bugarcic, T.; Habtemariam, A.; Stepankova, J.; Heringova, P.; Kasparkova, J.; Deeth, R. J.; Johnstone, R. D. L.; Prescimone, A.; Parkin, A.; Parsons, S.; Brabec, V.; Sadler, P. J.; *Inorg. Chem.* **2008**, *47*, 11470.

26. Colina-Vegas, L.; Dutra, J. L.; Villarreal, W.; Honorato, J.; Cominetti, M. R.; Pavan, F.; Navarro, M.; Batista, A. A.; *J. Inorg. Biochem.* **2016**, *162*, 135.

27. Higuera-Padilla, A. R.; Batista, A. A.; Colina-Vegas, L.; Villarreal, W.; Colnago, L. A.; *J. Coord. Chem.* **2017**, *70*, 3541.

28. Jensen, S. B.; Rodger, S. J.; Spicer, M. D.; *J. Organomet. Chem.* **1998**, *556*, 151.

29. Dowson, G. R. M.; Haddow, M. F.; Lee, J.; Wingad, R. L.; Wass, D. F.; *Angew. Chem., Int. Ed.* **2013**, *52*, 9005.

30. Lalrempuia, R.; Carroll, P. J.; Kollipara, M. R.; *J. Coord. Chem.* **2003**, *56*, 1499.

31. Daguenet, C.; Scopelliti, R.; Dyson, P. J.; *Organometallics* **2004**, *23*, 4849.

32. Kissounko, D. A.; Kissounko, N. S.; Krut'Ko, D. P.; Brusova, G. P.; Lemenovskii, D. A.; Boag, N. M.; *J. Organomet. Chem.* **1998**, *556*, 145.

33. Cunha, B. N.; Colina-Vegas, L.; Plutín, A. M.; Silveira, R. G.; Honorato, J.; Oliveira, K. M.; Cominetti, M. R.; Ferreira, A. G.; Castellano, E. E.; Batista, A. A.; *J. Inorg. Biochem.* **2018**, *186*, 147.

34. Colina-Vegas, L.; Luna-Dulcey, L.; Plutín, A. M.; Castellano, E. E.; Cominetti, M. R.; Batista, A. A.; *Dalton Trans.* **2017**, *46*, 12865.

35. Kandioller, W.; Balsano, E.; Meier, S. M.; Jungwirth, U.; Göschl, S.; Roller, A.; Jakupec, M. A.; Berger, W.; Keppler, B. K.; Hartinger, C. G.; *Chem. Commun.* **2013**, *49*, 3348.

36. Tabrizi, L.; Chiniforoshan, H.; *J. Organomet. Chem.* **2016**, *822*, 211.

37. Mandal, P.; Kundu, B. K.; Vyas, K.; Sabu, V.; Helen, A.; Dhankhar, S. S.; Nagaraja, C. M.; Bhattacherjee, D.; Bhabak, K. P.; Mukhopadhyay, S.; *Dalton Trans.* **2018**, *47*, 517.

38. Tabares, J. P. G.; Santos, R. L. S. R.; Cassiano, J. L.; Zaim, M. H.; Honorato, J.; Batista, A. A.; Teixeira, S. F.; Ferreira, A. K.; Viana, R. B.; Martínez, S. Q.; Stábile, A. C.; Silva, D. O.; *Inorg. Chim. Acta* **2019**, *489*, 27.

39. Sinopalnikova, I. S.; Peganova, T. A.; Novikov, V. V.; Fedyanin, I. V.; Filippov, O. A.; Belkova, N. V.; Shubina, E. S.; Poli, R.; Kalsin, A. M.; *Chem. - Eur. J.* **2017**, *23*, 15424.

40. Dougan, S. J.; Melchart, M.; Habtemariam, A.; Parsons, S.; Sadler, P. J.; *Inorg. Chem.* **2006**, *45*, 10882.

41. Honorato, J.; Colina-Vegas, L.; Correa, R. S.; Guedes, A. P. M.; Miyata, M.; Pavan, F. R.; Ellena, J.; Batista, A. A.; *Inorg. Chem. Front.* **2019**, *6*, 376.

42. Nakamoto, K.; *Infrared and Raman Spectra of Inorganic and Coordination Compounds: Part B: Applications in Coordination, Organometallic, and Bioinorganic Chemistry*, 6th ed.; John Wiley & Sons: Hoboken, New Jersey, 2008.

43. Nakamoto, K.; *Infrared and Raman Spectra of Inorganic and Coordination Compounds: Part A, Theory and Applications in Inorganic Chemistry*; Wiley: Hoboken, 2009.

44. Lopes, J. C. S.; Damasceno, J. L.; Oliveira, P. F.; Guedes, A. P. M.; Tavares, D. C.; Deflon, V. M.; Lopes, N. P.; Pivatto, M.; Batista, A. A.; Maiag, P. I. S.; Von Poelhsitz, G.; *J. Braz. Chem. Soc.* **2015**, *26*, 1838.

45. Graminha, A. E.; Honorato, J.; Dulcey, L. L.; Godoy, L. R.; Barbosa, M. F.; Cominetti, M. R.; Menezes, A. C.; Batista, A. A.; *J. Inorg. Biochem.* **2020**, *206*, 111021.

46. Amass, A. J.; Brough, P. E.; Colclough, M. E.; Philbin, I. M.; Perry, M. C.; *Des. Monomers Polym.* **2004**, *7*, 413.

47. Viesser, R. V.; Ducati, L. C.; Tormena, C. F.; Autschbach, J.; *Chem. Sci.* **2017**, *8*, 6570.

48. Biancalana, L.; Pampaloni, G.; Zacchini, S.; Marchetti, F.; *J. Organomet. Chem.* **2018**, *869*, 201.

49. Timm, M.; Saaby, L.; Moesby, L.; Hansen, E. W.; *Cytotechnology* **2013**, *65*, 887.

50. Jamalzadeh, L.; Ghafoori, H.; Sariri, R.; Rabuti, H.; Nasirzade, J.; Hasani, H.; Aghamaali, M. R.; *Avicenna J. Med. Biochem.* **2016**, *4*, 10.

51. Renier, O.; Deacon-Price, C.; Peters, J.; Nurekeyeva, K.; Russon, C.; Dyson, S.; Ngubane, S.; Baumgartner, J.; Dyson, P.; Riedel, T.; Chiririwa, H.; Blom, B.; *Inorganics* **2017**, *5*, 44.

52. Biancalana, L.; Zacchini, S.; Ferri, N.; Lupo, M. G.; Pampaloni, G.; Marchetti, F.; *Dalton Trans.* **2017**, *46*, 16589.

53. Abbro, L.; Dini, L.; *Ital. J. Zool.* **2003**, *70*, 297.

54. Rahman, S. N. S. A.; Wahab, N. A.; Malek, S. N. A.; *Evidence-Based Complementary Altern. Med.* **2013**, *2013*, 257108.

55. Richter, V.; Voit, F.; Kienle, A.; Schneckenburger, H.; *J. Microsc.* **2015**, *257*, 1.

56. Wen, Y.; Chen, Z.; Lu, J.; Ables, E.; Scemama, J.-L.; Yang, L. V.; Lu, J. Q.; Hu, X.-H.; *PLoS One* **2017**, *12*, e0184726.

57. Ribeiro, G. H.; Colina-Vegas, L.; Clavijo, J. C. T.; Ellena, J.; Cominetti, M. R.; Batista, A. A.; *J. Inorg. Biochem.* **2019**, *193*, 70.

58. Munshi, A.; Hobbs, M.; Meyn, R. E. In *Chemosensitivity*, vol. 110; Blumenthal, R. D., ed.; Humana Press: New Jersey, 2005, p. 021-028.

59. Franken, N. A. P.; Rodermond, H. M.; Stap, J.; Haveman, J.; van Bree, C.; *Nat. Protoc.* **2006**, *1*, 2315.

60. de Grandis, R. A.; dos Santos, P. W. S.; de Oliveira, K. M.; Machado, A. R. T.; Aissa, A. F.; Batista, A. A.; Antunes, L. M. G.; Pavan, F. R.; *Bioorg. Chem.* **2019**, *85*, 455.

61. Villarreal, W.; Colina-Vegas, L.; de Oliveira, C. R.; Tenorio, J. C.; Ellena, J.; Gozzo, F. C.; Cominetti, M. R.; Ferreira, A. G.; Ferreira, M. A. B.; Navarro, M.; Batista, A. A.; *Inorg. Chem.* **2015**, *54*, 11709.

62. Antonarakis, E. S.; Emadi, A.; *Cancer Chemother. Pharmacol.* **2010**, *66*, 1.

63. Colina-Vegas, L.; Oliveira, K.; Cunha, B.; Cominetti, M.; Navarro, M.; Batista, A. A.; *Inorganics* **2018**, *6*, 132.

64. Blunden, B. M.; Lu, H.; Stenzel, M. H.; *Biomacromolecules* **2013**, *14*, 4177.

65. Egger, A. E.; Rappel, C.; Jakupec, M. A.; Hartinger, C. G.; Heffeter, P.; Keppler, B. K.; *J. Anal. At. Spectrom.* **2009**, *24*, 51.

66. Chen, L. M.; Peng, F.; Li, G. D.; Jie, X. M.; Cai, K. R.; Cai, C.; Zhong, Y.; Zeng, H.; Li, W.; Zhang, Z.; Chen, J. C.; *J. Inorg. Biochem.* **2016**, *156*, 64.

67. Robertson, D. R.; Robertson, I. W.; Stephenson, T. A.; *J. Organomet. Chem.* **1980**, *202*, 309.

68. Bennett, M. A.; Smith, A. K.; *J. Chem. Soc., Dalton Trans.* **1974**, 233.

69. Sheldrick, G. M.; IUCr; *Acta Crystallogr., Sect. A: Found. Adv.* **2015**, *71*, 3.

70. Dolomanov, O. V.; Bourhis, L. J.; Gildea, R. J.; Howard, J. A. K.; Puschmann, H.; *J. Appl. Crystallogr.* **2009**, *42*, 339.

71. Macrae, C. F.; Bruno, I. J.; Chisholm, J. A.; Edgington, P. R.; McCabe, P.; Pidcock, E.; Rodriguez-Monge, L.; Taylor, R.; Van De Streek, J.; Wood, P. A.; *J. Appl. Crystallogr.* **2008**, *41*, 466.